10

Crystal structure, luminescence properties and thermometric characteristics of $Ba_2Gd_2Ge_4O_{13}$:Tb^{3+}, Tb^{3+}/Eu^{3+} germanates

© A.V. Chvanova, O.A. Lipina, A.Yu. Chufarov, A.P. Tyutyunnik, L.L. Surat, V.G. Zubkov

Institute of Solid State Chemistry, Russian Academy of Sciences, Ural Branch, Yekaterinburg, Russia

e-mail: chvanova10_99@mail.ru

Received April 15, 2024
Revised May 27, 2024
Accepted May 27, 2024

In this work, the synthesis of $Ba_2Gd_{2-x}Tb_xGe_4O_{13}$ $(x = 0.05 - 0.2)$ and $Ba_2Gd_{1.85-y}Tb_{0.15}Eu_yGe_4O_{13}$ $(y = 0.1 - 0.6)$ solid solutions was carried out for the first time and the crystal structure of the synthesized phases was studied. The XRPD study has verified that all the samples are isostructural to $Ba_2Gd_2Ge_4O_{13}$ and crystallize in the monoclinic system, S.G. $C2/c$, $Z = 4$. The photoluminescence spectra of $Ba_2Gd_{2-x}Tb_xGe_4O_{13}$ germanates consist of a number of lines in the range of 365−650 nm, caused by $^5D_{3,4} \rightarrow {}^7F_J$ transitions in Tb^{3+} ions. Based on the results of concentration studies, it has been found that $Ba_2Gd_{1.85}Tb_{0.15}Ge_4O_{13}$ germanate exhibits the highest emission intensity. This content of Tb^{3+} $(x = 0.15)$ was fixed and the codoped $Ba_2Gd_{1.85-y}Tb_{0.15}Eu_yGe_4O_{13}$ phases were synthesized. Codoping with Eu^{3+} ions has led to the appearance of additional luminescent lines in the 570−720 nm region, which is associated with $^5D_0 \rightarrow {}^7F_J$ transitions in europium ions. As the Eu^{3+} content increases, the color coordinates gradually change, which allows fine-tuning of the emission color of the phosphors. High-temperature studies $(T = 298-498\,\mathrm{K})$ were carried out for $Ba_2Gd_{1.75}Tb_{0.15}Eu_{0.1}Ge_4O_{13}$ germanate. The temperature dependences of the luminescence of the bands at 530−560 nm ($^5D_4 \rightarrow {}^7F_5$ transition in Tb^{3+}) and 603−640 nm ($^5D_0 \rightarrow {}^7F_2$ transition in Eu^{3+}) as well as $I_{603-640\,\mathrm{nm}}/I_{530-560\,\mathrm{nm}}$ were plotted. The calculated maximum values of absolute and relative sensitivity were $0.34\% \times \mathrm{K}^{-1}$ and $0.15\% \times \mathrm{K}^{-1}$.

Keywords: luminescence, germanate, europium, terbium, thermometry.

DOI: 10.61011/EOS.2024.06.59535.6268-24

Introduction

Development of the methods allowing accurate remote temperature measurement in nanoscale items is currently a key challenge for microelectronics, microoptics and photonics [1]. It is difficult to use traditional contact sensors (for example, thermistors and thermocouples) when the size of an item is not larger than $1\,\mu$m, because temperature equilibrium is set due to the contact between the sensor and item during temperature measurement, which leads to distortion of measurements. Creation of luminescent thermometers, whose main advantages are noninvasiveness, high accuracy, measurement in corrosive media and adverse conditions, and micro/nanoscale applicability, is a very promising research area [1–5]. Operating principle of the luminescent sensor is based on the measurement of temperature-dependent optical parameters, which may include width, intensity or position of the emission band in the photoluminescence spectra, lifetime of the excited state, luminescence intensity ratio (LIR) of two emission bands [1–3].

In case of LIR thermometry, emission bands detected in the luminescence spectra of compounds activated by the Er^{3+}, Tm^{3+}, Ho^{3+}, Dy^{3+}, Eu^{3+}, Sm^{3+}, Nd^{3+} or Pr^{3+} ions often serve as the analytical lines [1,2,4,6–11]. LIR value varies due to partial intracenter transitions from one excited state 1 to overlying thermally-coupled excited state 2, whereby $LIR = f(T)$ may be described [1,2] by equation

$$LIR = A\exp(-\Delta E_{21}/k_\mathrm{B}T), \quad (1)$$

where A is the constant, ΔE_{21} is the energy gap between two states of an ion, k_B is the Boltzmann constant, T is the temperature.

It should be noted that to perform the thermally induced transition $1 \rightarrow 2$, ΔE_{21} shall not exceed $2000\,\mathrm{cm}^{-1}$, which imposes restrictions on the maximum absolute and relative sensitivities [1–6,11,12]:

$$S_a = \mathrm{d}LIR/\mathrm{d}T = (\Delta E_{21}/k_\mathrm{B}T^2)[A\exp(-\Delta E/k_\mathrm{B}T)], \quad (2)$$

$$S_r = (1/LIR)(\mathrm{d}LIR/\mathrm{d}T) = \Delta E_{21}/k_\mathrm{B}T^2. \quad (3)$$

This restriction may be overcome by means of introduction of additional luminescent ions into the phosphor composition and determination of the intensity ratio of bands induced by transitions from thermally uncoupled levels of two different centers. Oxygen-containing hosts codoped with the Bi^{3+}/Sm^{3+}, Bi^{3+}/Eu^{3+}, Bi^{3+}/Dy^{3+}, Bi^{3+}/Tb^{3+}, Tb^{3+}/Eu^{3+}, Tb^{3+}/Pr^{3+} ions, having high thermal stability, chemical resistance and high temperature-sensing properties shall be primarily highlighted among the candidates for temperature measurement applications [13–23]. Moreover, in phosphors activated by two and more types of ions, fine tuning of emission color is possible by varying the dopant concentration. The Eu^{3+} and Tb^{3+} ions are the most frequently used

activators due to their characteristic emission in the range of 480−650 and 570−720 nm, respectively. Excitation in both cases is induced by UV radiation [24]. The existing literature provides data on the luminescence properties of $Y_2BaAl_4SiO_{12}$:Tb^{3+}/Eu^{3+}, $Li_3Lu_3Te_2O_{12}$:Tb^{3+}/Eu^{3+}, $NaCaGd(WO_4)_3$:Tb^{3+}/Eu^{3+} [25–27], that are promising phosphors with tunable color characteristics and may be used for creation of white light-emitting diodes (wLED).

This study has investigated the crystal structure and optical properties of $Ba_2Gd_2Ge_4O_{13}$:Tb^{3+}, Tb^{3+}/Eu^{3+}. The influence of dopant concentration, exciting radiation wavelength and temperature on the luminescence properties of the powders has been found. Note that the features of crystal structure of $Ba_2RE_2Ge_4O_{13}$ (RE = Pr, Nd, Eu, Gd, Dy, Y) tetragermanates were analyzed for the first time in [28–30]. The results of X-ray powder diffraction studies have shown that the lattice of the compounds consists of $[Ge_4O_{13}]$ groups, $[RE_2O_{12}]$ dimers and barium atoms coordinated by ten oxygen atoms. The authors of [30] demonstrated high temperature resistance of the luminescence properties of $Ba_2Gd_2Ge_4O_{13}$:Dy^{3+} and $Ba_2Y_2Ge_4O_{13}$:Dy^{3+}. During heating to 423 K, reduction of luminescence intensity was not higher than 10% of the initial value measured at room temperature and the shift of color coordinates was just $\Delta x \leq 0.0055$ and $\Delta y \leq 0.0050$. In [7], potential use of $Ba_2Gd_2Ge_4O_{13}$ activated by the Sm^{3+} ions as a material for a sensing element of a non contact temperature sensor was studied. The findings showed that the phosphor has high relative sensitivity, $S_r(\max) = 1.57\% \times K^{-1}$, and there is a good reproducibility of the obtained LIR values. All of the aforesaid indicates that promising phosphors may be created on the basis of $Ba_2RE_2Ge_4O_{13}$ for light-emitting diodes as well as for non contact temperature measurements.

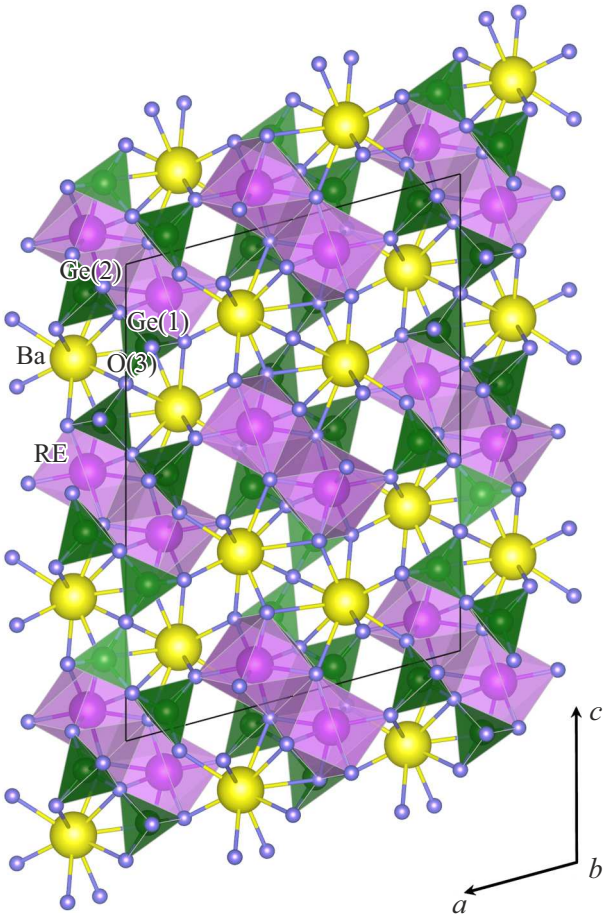

Figure 1. General view of $Ba_2Gd_{2-x}Tb_xGe_4O_{13}$ and $Ba_2Gd_{1.85-y}Tb_{0.15}Eu_yGe_4O_{13}$ crystal structures along [010] orientation.

Materials and methods

$Ba_2Gd_{2-x}Tb_xGe_4O_{13}$ $(x = 0.05 - 0.2)$ and $Ba_2Gd_{1.85-y}Tb_{0.15}Eu_yGe_4O_{13}$ $(y = 0.1 - 0.6)$ were obtained by the solid state method. The following substances were used for the synthesis of the powders: $BaCO_3$ (99.9%), Gd_2O_3 (99.999%), Tb_4O_7 (99.998%), Eu_2O_3 (99.99%), GeO_2 (99.9%). Tb_4O_7 was preliminary reduced to Tb_2O_3 by annealing in Ar/H_2 flux at 1573 K during 24h. The initial oxides and barium carbonate taken in stoichiometric quantities were mixed in a mortar and thoroughly ground with addition of ethanol, and then stage annealed in 100 K steps from 1073 K to 1473 K . Intermediate grindings were performed after each synthesis stage.

X-ray diffraction analysis of the synthesized compounds was performed using the STADI-P (STOE) diffractometer equipped with a linear position-sensitive detector. The record was performed in Cu$K_{\alpha 1}$-radiation in 0.02° steps in the angle range $2\theta = 5° - 120°$. Polycrystalline silicon with the lattice cell parameter $a = 5.43075(5)$ Åwas used as an internal standard. Structure refinement was performed in PowderCell 2.4 [31] using data for $Ba_2Gd_2Ge_4O_{13}$ [29].

Photoluminescence spectra and excitation photoluminescence spectra of the samples as well as photoluminescence decay curves were measured using the Cary Eclipse (Varian, USA) fluorescent pulsed spectrophotometer: excitation source — 75 kW pulsed Xenon lamp, detector — PMT R928. Measurements in the range of 298−498 K were conducted using the GS-21525 (Specac Ltd, UK) thermostat with optical windows.

Results and discussion

Description of crystal structure

The results of X-ray diffraction analysis have shown that $Ba_2Gd_{2-x}Tb_xGe_4O_{13}$ $(x = 0.05 - 0.2)$ and $Ba_2Gd_{1.85-y}Tb_{0.15}Eu_yGe_4O_{13}$ $(y = 0.1 - 0.6)$ solid solutions crystallize in a monoclinic crystal system, space group $C2/c$, $Z = 4$. All compounds are isostructural to $Ba_2Gd_2Ge_4O_{13}$. Proximity of crystal radii of the Gd^{3+} $(CR = 1.14$ Å), Tb^{3+} $(CR = 1.12$ Å) and Eu^{3+}

Table 1. Crystal lattice parameters for solid solutions $Ba_2Gd_{2-x}Tb_xGe_4O_{13}$ and $Ba_2Gd_{1.85-y}Tb_{0.15}Eu_yGe_4O_{13}$

Dopant concentration	a, Å	b, Å	c, Å	β	V, Å^3
$Ba_2Gd_{2-x}Tb_xGe_4O_{13}$					
0.05	13.0751(4)	5.3667(2)	17.9938(6)	105.086(2)°	1219.11(7)
0.1	13.0743(5)	5.3668(2)	17.9924(8)	105.083(4)°	1218.98(10)
0.15	13.0736(8)	5.3665(3)	17.9922(12)	105.091(4)°	1218.79(14)
0.2	13.0726(5)	5.3677(2)	17.9902(8)	105.146(3)°	1218.52(9)
$Ba_2Gd_{1.85-y}Tb_{0.15}Eu_yGe_4O_{13}$					
0.1	13.0732(4)	5.3654(2)	17.9897(6)	105.086(3)°	1218.36(7)
0.2	13.0710(3)	5.3691(2)	17.9925(7)	105.168(2)°	1218.72(7)
0.3	13.0757(5)	5.3676(2)	17.9919(7)	105.111(3)°	1219.11(8)
0.4	13.0783(5)	5.3694(2)	17.9951(8)	105.142(3)°	1219.79(9)
0.5	13.0765(4)	5.3694(2)	17.9944(7)	105.141(2)°	1219.57(7)
0.6	13.0814(5)	5.3679(2)	17.9918(8)	105.090(3)°	1219.82(9)

($CR = 1.15$ Å) ions [32] suggests that the dopant ions occupy the gadolinium positions in the $Ba_2Gd_2Ge_4O_{13}$ lattice. As can be seen from the data listed in Table 1, as the concentration of Tb^{3+} increases, lattice cell parameters and volume of the $Ba_2Gd_{2-x}Tb_xGe_4O_{13}$ phases gradually decrease, while substitution of the Gd^{3+} ions by the Eu^{3+} ions in $Ba_2Gd_{1.85-y}Tb_{0.15}Eu_yGe_4O_{13}$ facilitates gradual increase in the lattice cell parameters and volume.

The crystal structure of the synthesized compounds is shown in Figure 1. All atoms occupy common positions, except the O(3) atoms through which the a two-fold rotation axis goes parallel to [010] direction. The O(3) atoms are bridging atoms that interconnect two equivalent fragments of the Ge_4O_{13} tetragroup. Rare earth atoms are coordinated by seven oxygen atoms and form RE_2O_{12} dimers. By interconnecting through the GeO_4 tetrahedra, they form a heteropolyhedral framework. The Ba atoms occupy the voids between polyhedra (coordination number is 10).

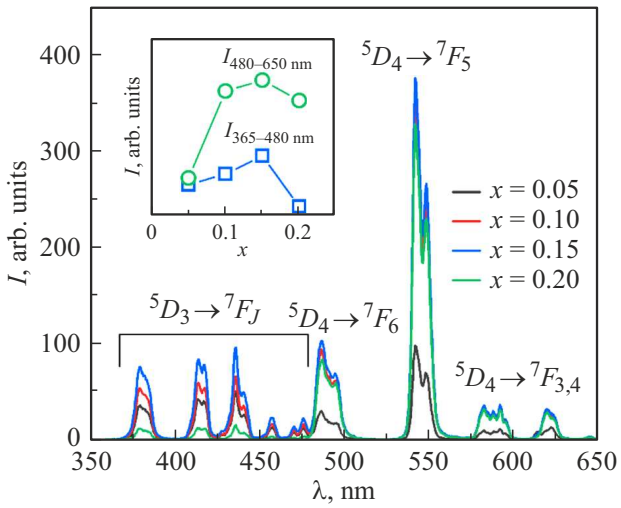

Figure 2. Luminescence spectra ($\lambda_{ex} = 312$ nm) of the $Ba_2Gd_{2-x}Tb_xGe_4O_{13}$ samples. Inset — dependences of the emission intensity on concentration in the ranges of 365–480 and 480–650 nm.

Luminescence properties of $Ba_2Gd_{2-x}Tb_xGe_4O_{13}$

Under UV radiation ($\lambda_{ex} = 312$ nm), $Ba_2Gd_{2-x}Tb_xGe_4O_{13}$ luminesce in the range of 365–650 nm (Figure 2). The most intense line for all samples is located at 530–560 nm and caused by the $^5D_4 \rightarrow {}^7F_5$ transition in the Tb^{3+} ions. Some bands with maxima at 487, 583 and 620 nm are also caused by intracenter transitions from the excited $^5D_4$ level. Additionally, the photoluminescence spectra of $Ba_2Gd_{2-x}Tb_xGe_4O_{13}$ contain peaks in the short-wavelength range of spectrum connected with $^5D_3 \rightarrow {}^7F_6$ (379 nm), $^5D_3 \rightarrow {}^7F_5$ (416 nm), $^5D_3 \rightarrow {}^7F_4$ (437 nm) and $^5D_3 \rightarrow {}^7F_3$ (462 nm) transitions. Investigations of the dependence on concentration have shown that the $Ba_2Gd_{1.85}Tb_{0.15}Ge_4O_{13}$ sample has the highest luminescence intensity, while for germanate with the maximum dopant concentration ($x = 0.2$), luminescence intensity reduction is observed throughout the examined wavelength range due to concentration quenching and cross-relaxation process: $^5D_3(Tb^{3+}) + {}^7F_6(Tb^{3+}) \rightarrow {}^5D_4(Tb^{3+}) + {}^7F_0(Tb^{3+})$, that is described in detail in [33].

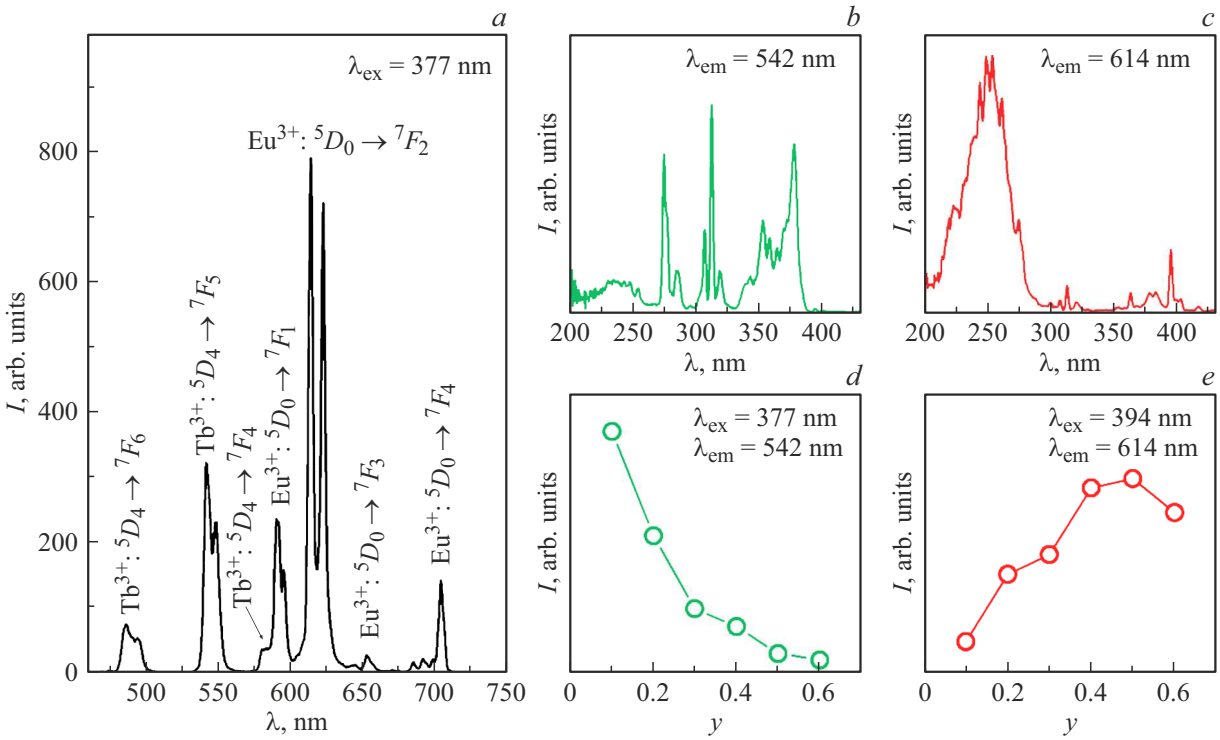

Figure 3. Luminescence spectrum of germanate $Ba_2Gd_{1.75}Tb_{0.15}Eu_{0.1}Ge_4O_{13}$, $\lambda_{ex} = 377$ nm (*a*); excitation spectra $Ba_2Gd_{1.75}Tb_{0.15}Eu_{0.1}Ge_4O_{13}$, $\lambda_{em} = 542$ (*b*), 614 nm (*c*); dependences of integral line intensity at 542 (*d*) and 614 nm on concentration (*e*).

Luminescence properties of $Ba_2Gd_{1.85-y}Tb_{0.15}Eu_yGe_4O_{13}$

As an example, Figure 3, *a* shows the luminescence spectrum of the $Ba_2Gd_{1.75}Tb_{0.15}Eu_{0.1}Ge_4O_{13}$ sample recorded in the range of 460–750 nm measured under radiation with $\lambda_{ex} = 377$ nm. It can be seen that doping of $Ba_2Gd_{1.85}Tb_{0.15}Ge_4O_{13}$ with the Eu^{3+} ions leads to appearance of additional bands in the luminescence spectra within 570–720 nm associated with the transitions from the excited $^5D_0$-level to the ^7F_J levels $(J = 0 - 4)$ in the Eu^{3+} ions. Figure 3, *b, c* shows excitation spectra of the sample obtained by monitoring the radiation with $\lambda_{em} = 542$ nm (transition $^5D_4 \rightarrow {}^7F_5$ in Tb^{3+}) and 614 nm (transition $^5D_0 \rightarrow {}^7F_2$ in Eu^{3+}). Note that spectrum shape significantly depends on the chosen λ_{em}. The excitation spectrum obtained by monitoring the emission at 542 nm (Figure 3, *b*) contains a wide band at 200–260 nm. The suggested excitation mechanism in this range is most probably connected with charge transfer from the oxygen ions to the europium ions and subsequent energy transfer to the Tb^{3+} ions. In addition, the specified wavelength range may contain bands connected with spin-allowed electronic transitions $4f^8(^7F_6) \rightarrow 4f^7(^8S)5d(^7D)$ in the Tb^{3+} ions. Some narrow peaks at 270–330 nm correspond to the $^8S_{7/2} \rightarrow {}^6D_{7/2}$ and $^8S_{7/2} \rightarrow {}^6I_{9/2}$ transitions in the Gd^{3+} ions; their existence and high intensity indicate that the energy transfer from Gd^{3+} to Tb^{3+} is very effective. The fact that the Gd^{3+} ions absorb and effectively transfer energy to the codopant ions additionally demonstrates that excitation of samples by radiation with $\lambda_{ex} = 275$ nm is not followed by emission at 300–320 nm (transition $^6P_{7/2} \rightarrow {}^8S_{7/2}$ in the Gd^{3+} ions). Luminescence sensitization of Tb^{3+} ions by the Gd^{3+} ions was previously observed for the phosphors: $Na_3Gd(BO_3)_2$:Tb^{3+}, $LaAlGe_2O_7$:Gd^{3+}, Tb^{3+}, (La,Gd)PO_4:Tb^{3+} [34–36]. In the long-wavelength range of the excitation spectrum (330–390 nm), there is also a wide band corresponding to $4f \rightarrow 4f$ transitions in the Tb^{3+} ions: $^7F_6 \rightarrow {}^5L_9$ (352 nm), $^7F_6 \rightarrow {}^5L_{10}$ (364 nm) and $^7F_6 \rightarrow {}^5D_3$ (377 nm). The excitation spectrum obtained by monitoring the emission with $\lambda_{em} = 614$ nm (Figure 3, *c*) contain a wide intense charge transfer band and a set of narrow peaks associated with the transitions $4f \rightarrow 4f$ in the Gd^{3+}, Tb^{3+} and Eu^{3+} ions: $^8S_{7/2} \rightarrow {}^6I_{9/2}$ (275 nm, Gd^{3+}), $^8S_{7/2} \rightarrow {}^6P_{7/2}$ (312 nm, Gd^{3+}), $^7F_0 \rightarrow {}^5D_4$ (362 nm, Eu^{3+}), $^7F_6 \rightarrow {}^5D_3$ (377 nm, Tb^{3+}), $^7F_0 \rightarrow {}^5L_7$ (381 nm, Eu^{3+}), $^7F_0 \rightarrow {}^5L_6$ (394 nm, Eu^{3+}), $^7F_0 \rightarrow {}^5D_3$ (393 nm, Eu^{3+}).

Investigations of the dependence on concentration show that the increase in codopant concentration in the $Ba_2Gd_{1.85-y}Tb_{0.15}Eu_yGe_4O_{13}$ phases leads to the gradual decrease in the luminescence intensity in the range of 480–560 nm, while the luminescence intensity in the range of 570–720 nm increases and achieves its maximum value at $y = 0.5$ (Figure 3, *d, e*). Thus, targeted tuning of emission color may be performed by varying the content of Eu^{3+}. During further investigations, the excitation of the samples was carried out by radiation with $\lambda_{ex} = 377$ nm, because in this case intense luminescence of

Table 2. Color parameters of phosphors $Ba_2Gd_{1.85-y}Tb_{0.15}Eu_yGe_4O_{13}$ ($y = 0.1 - 0.6$), $\lambda_{ex} = 377$ nm

y	chromaticity coordinates	CCT
0.1	(0.528; 0.426)	2056
0.2	(0.603; 0.378)	1649
0.3	(0.634; 0.357)	1988
0.4	(0.648; 0.347)	2308
0.5	(0.654; 0.343)	2473
0.6	(0.656; 0.341)	2552

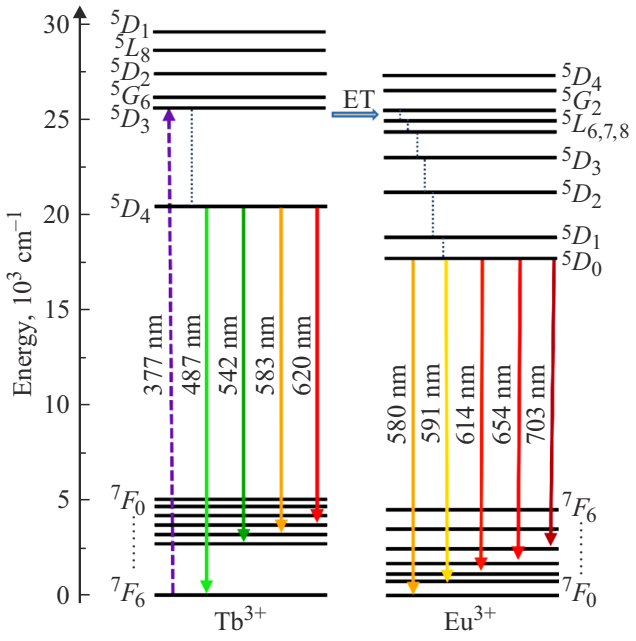

Figure 4. Energy level diagrams of the Tb^{3+}, Eu^{3+} ions and energy transfer in phosphors $Ba_2Gd_{1.85-y}Tb_{0.15}Eu_yGe_4O_{13}$.

the $Ba_2Gd_{1.85-y}Tb_{0.15}Eu_yGe_4O_{13}$ samples was achieved in a wide wavelength range. For $Ba_2Gd_{1.85-y}Tb_{0.15}Eu_yGe_4O_{13}$ phosphors, chromaticity coordinates and correlated color temperature (CCT) were determined in comparison with International Standard CIE 1931. The correlated color temperature was calculated [37] using the following equation

$$\mathrm{CCT} = -449n^3 + 3525n^2 - 6823.3n + 5520.33, \qquad (4)$$

$$n = \frac{x - x_e}{y - y_e}, \qquad (5)$$

where x_e and y_e are „epicenter" coordinates in the chromaticity diagram of a white light source equal to 0.332 and 0.1858, respectively, x and y are the chromaticity coordinates of the test sample. The obtained data is summarized in Table 2.

Energy level diagrams of the $Tb^{3+}$and Eu^{3+} ions are shown in Figure 4. When germanates are excited by 377 nm radiation, the Tb^{3+} ions are initially excited and transfer from the ground state $^7F_6$ to the excited $^5D_3$ state. Then, nonradiative relaxation or cross-relaxation $^5D_3(Tb^{3+}) + {}^7F_6(Tb^{3+}) \rightarrow {}^5D_4(Tb^{3+}) + {}^7F_0(Tb^{3+})$ results in filling the $^5D_4$ state. Transition from this state to the underlying $^7F_{3,4,5,6}$ levels leads to appearance of emission at 480−650 nm. At the same time, energy transfer from Tb^{3+} to Eu^{3+} may be possible because the excitation and emission region of the Tb^{3+}ions overlaps with the excitation region of the Eu^{3+} ions [38]. As a results of further nonradiative transitions, the $^5D_0$ level is filled in the Eu^{3+} ions, transition from this level to the underlying ^7F_J levels leads to luminescence in the range of 570−720 nm.

Figure 5, *a* shows the luminescence spectra of $Ba_2Gd_{1.75}Tb_{0.15}Eu_{0.1}Ge_4O_{13}$ recorded with stage heating up to 473 K. As can be seen from the shown spectra, the luminescence intensity gradually decreases throughout the investigated wavelength range as the temperature grows. It should be noted that the intensity of luminescent lines caused by the electronic transitions in different types of ions decreases unevenly (Figure 5, *b*). At $T = 473$ K, band intensity in the range of 603−640 nm (transition in Eu^{3+}) is 69.9% of the initial value, while band intensity in the range of 530−560 nm (transition in Tb^{3+}) is 62.5%. Figure 5, *c* shows how $\mathrm{LIR} = I_{603-640\,\mathrm{nm}}(Eu^{3+})/I_{530-560\,\mathrm{nm}}(Tb^{3+})$ varies with temperature. The obtained dependence is adequately described ($R_2 \geq 99.7\%$) by the following equation [39,40]:

$$LIR = \frac{I_{Eu}}{I_{Tb}} = \frac{I_{0Eu}\left[1 + C_{Tb}\exp\left(\frac{-\delta E_{Eu}}{k_B T}\right)\right]}{I_{0Tb}\left[1 + C_{Eu}\exp\left(\frac{-\Delta E_{Tb}}{k_B T}\right)\right]}, \qquad (6)$$

where I_{0Eu} and I_{0Tb} are initial intensities of the corresponding lines, C_{Eu} and C_{Tb} are constants, ΔE_{Eu} and ΔE_{Tb} are the temperature quenching activation energies, k_B is the Boltzmann constant, T is the temperature.

Dependences of the relative and absolute sensitivities are shown in Figure 5, *d, e*. Relative and absolute sensitivities decrease with temperature.

Absolute and relative sensitivities of temperature measurement for the $Ba_2Gd_{1.75}Tb_{0.15}Eu_{0.1}Ge_4O_{13}$ sample were evaluated from equations (2), (3). All obtained values of S_a and S_r are listed in Table 3 together with previously published data for compounds doped with Eu^{3+}/Tb^{3+} [19–23]. According to the obtained results, the maximum values of S_a and S_r equal to 0.34 and $0.15\% \times K^{-1}$, respectively, are achieved at 298 K. The obtained absolute sensitivity values do not imply that $Ba_2Gd_{1.75}Tb_{0.15}Eu_{0.1}Ge_4O_{13}$ may be used as a material for non contact temperature measurement, however, stability of color characteristcs of the sample is suggested.

At the final stage of the study, luminescence decay curves with $\lambda_{em} = 542$ and 614 nm were measured for

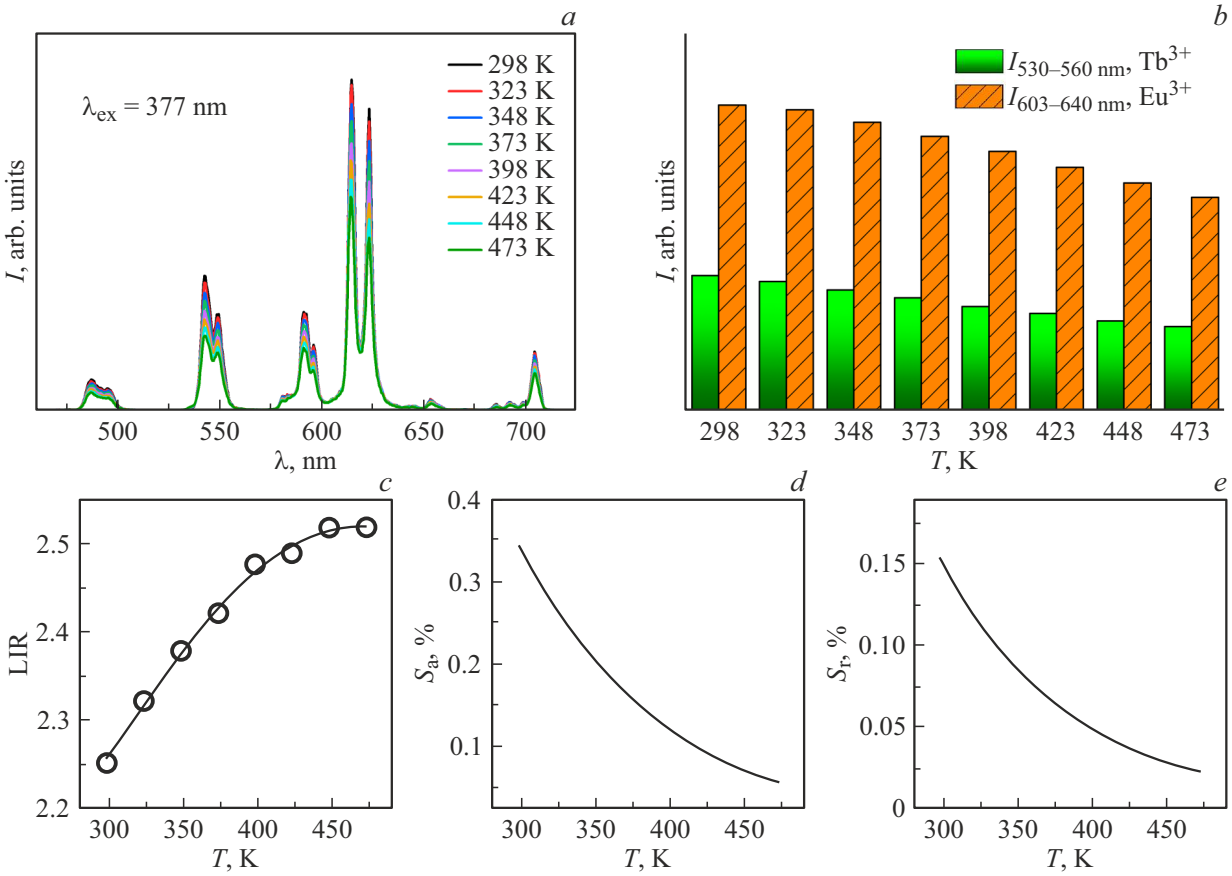

Figure 5. Luminescence spectra of $Ba_2Gd_{1.75}Tb_{0.15}Eu_{0.1}Ge_4O_{13}$, recorded at various heating temperatures (*a*); temperature dependences of integral intensities luminescent lines caused by the $^5D_0 \rightarrow {}^7F_2$ (603–640 nm) transitions in the Eu^{3+} ions and the $^5D_4 \rightarrow {}^7F_5$ (530–560 nm) transitions in the Tb^{3+} ions (*b*); temperature dependences of the intensity ratio of two analytical lines (*c*); temperature dependences of the absolute (S_a) and relative (S_r) sensitivities of temperature measurements (*d*, *e*).

Table 3. Temperature-sensing properties of various compounds activated by the Tb^{3+}/Eu^{3+} ions

Compound	S_a (max), % × K^{-1}	S_r (max), % × K^{-1}	Reference*T*-range, K	
$Ca_8ZnLa(PO_4)_7$:Tb^{3+}/Eu^{3+}	–	0.53	298–448	[19]
$BaY_2(MoO_4)$:Tb^{3+}/Eu^{3+}	6.02 (293 K)	1.06 (256 K)	89–293	[20]
Sr_3MoO_6:Tb^{3+}/Eu^{3+}	0.27	0.24	14–300	[21]
$Ca_2Al_2SiO_7$:Tb^{3+}/Eu^{3+}	0.54	1.17	303–483	[22]
Gd_2O_3:Tb^{3+}/Eu^{3+}	0.19	2.44 (473 K)	123–473	[23]
$Ba_2Gd_2Ge_4O_{13}$:Tb^{3+}/Eu^{3+}	0.34 (298 K)	0.15 (298 K)	298This study–473	

$Ba_2Gd_{1.75}Tb_{0.15}Eu_{0.1}Ge_4O_{13}$ (Figure 6). To describe all dependences, the following functions was used [41]:

$$I(t) = A_1 \exp\left(\frac{-t}{\tau_1}\right) + A_2 \exp\left(\frac{-t}{\tau_2}\right), \qquad (7)$$

where $I(t)$ is the luminescence intensity at time t, A_1 and A_2 are constants, τ_1 and τ_2 are the exponential component decay times.

The mean lifetime τ_{av}:

$$\tau_{av} = \frac{A_1\tau_1^2 + A_2\tau_2^2}{A_1\tau_1 + A_2\tau_2}, \qquad (8)$$

varied from 1.25 to 1.18 ms and from 1.46 to 1.32 ms for emission at 542 and 614 nm, respectively, which is attributed to the increase in the probability of non-radiative transitions with temperature growth.

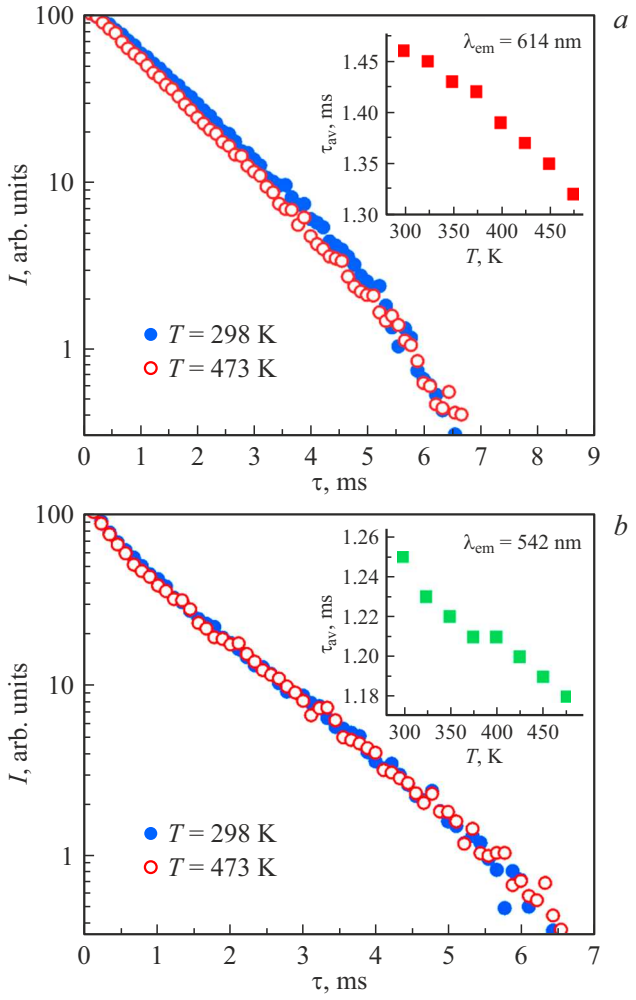

Figure 6. luminescence decay curves of phosphor $Ba_2Gd_{1.75}Tb_{0.15}Eu_{0.1}Ge_4O_{13}$ measured at 298 and 473 K, $\lambda_{em} = 614$ (*a*), 542 nm (*b*). Insets — τ_{av} vs. temperature.

Conclusions

$Ba_2Gd_{2-x}Tb_xGe_4O_{13}$ $(x = 0.05 - 0.2)$ and $Ba_2Gd_{1.85-y}Tb_{0.15}Eu_yGe_4O_{13}$ $(y = 0.1 - 0.6)$ were synthesized using a standard ceramic technique. According to the X-ray powder diffraction data, all compounds crystallize in the monoclinic crystal system, space group $C2/c$, $Z = 4$. Under UV radiation, germanates exhibit the luminesce in the range of 450–730 nm. The luminescence spectra of $Ba_2Gd_{1.85-y}Tb_{0.15}Eu_yGe_4O_{13}$ contain the typical peaks of the Eu^{3+} ions caused by transitions from the $^5D_0$ level to ^7F_J $(J = 0 - 4)$ states as well as peaks associated with transitions in the Tb^{3+} ions from the $^5D_4$ level to ^7F_J $(J = 3 - 6)$ states. It has been found that $Ba_2Gd_{1.75}Tb_{0.15}Eu_{0.1}Ge_4O_{13}$ has the maximum luminescence intensity in the range of 480–650 nm. Chromaticity coordinates and correlated color temperature have been calculated for all samples, the investigations have shown that $Ba_2Gd_{1.85-y}Tb_{0.15}Eu_yGe_4O_{13}$ phosphors are promising materials with adjustable emission color.

For the $Ba_2Gd_{1.75}Tb_{0.15}Eu_{0.1}Ge_4O_{13}$ sample, dependence of the optical characteristics from temperature has been studied. It has been found that the temperature increase leads to the growth of $I_{603-640\,nm}(Eu^{3+})/I_{530-560\,nm}(Tb^{3+})$. Calculated sensitivities reach the maximum values at room temperature and are equal to $0.34\% \times K^{-1}$ (S_a) and $0.15\% \times K^{-1}$ (S_r). For $Ba_2Gd_{1.75}Tb_{0.15}Eu_{0.1}Ge_4O_{13}$, luminescence decay curves have been also measured for radiation with $\lambda_{em} = 614$ nm (transition $^5D_0 \rightarrow ^7F_2$ in Eu^{3+}) and $\lambda_{em} = 542$ nm (transition $^5D_4 \rightarrow ^7F_5$ in Tb^{3+}), the calculated lifetime gradually decreases in both cases as the temperature grows.

Funding

The study of luminescent properties was supported by grant of the Russian Science Foundation №. 23-73-10090, https://rscf.ru/en/project/23-73-10090/. X-ray powder diffraction studies were performed under the state assignment of the Institute of Solid State Chemistry, Russian Academy of Sciences, Ural Branch, topic 124020600024-5.

Conflict of interest

The authors declare that they have no conflict of interest.

References

[1] C.D.S. Brites, A. Millán, L.D. Carlos. Handb. Phys. Chem. Rare Earths, **49**, 339–427 (2016). DOI: 10.1016/bs.hpcre.2016.03.005
[2] M. Dramićanin. *Lanthanide and Transition Metal Ion Doped Materials for Luminescence Temperature Sensing, Luminescence Thermometry: Methods, Materials, and Applications* (Woodhead Publishing Series in Electronic and Optical Materials, 2018), ch. 6, p. 113–157. DOI: 10.1016/B978-0-08-102029-6.00006-3
[3] V.K. Rai, S.B. Rai. Appl. Phys. B, **87**, 323–325 (2007). DOI: 10.1007/s00340-007-2592-z
[4] Y. Cui, F. Zhu, B. Chen, G. Qian. Chem. Commun., **51**, 7420–7431 (2015). DOI: 10.1039/c5cc00718f
[5] P. Du, J. Tang, W. Li, L. Luo. Chem. Eng. J., **406**, 127165 (2021). DOI: 10.1016/j.cej.2020.127165
[6] Q. Xiao, X. Yin, L. Lav, X. Dong, N. Zhou, K. Liu, X. Luo. J. Rare Earths, **41** (7), 981–988 (2023). DOI: 10.1016/j.jre.2022.04.013
[7] A.V. Chvanova, O.A. Lipina, A.Yu. Chufarov, A.P. Tyutyunnik, Ya.V. Baklanova, L.L. Surat, V.G. Zubkov. Russ. J. Inorg. Chem., **68**, 325–333 (2023). DOI: 10.1134/S003602362260246X
[8] O.A. Lipina, T.S. Spiridonova, Ya.V. Baklanova, E.G. Khaikina. Russ. J. Inorg. Chem., **68**, 529–537 (2023). DOI:10.1134/S0036023623600508
[9] O.A. Lipina, Ya.V. Baklanova, T.S. Spiridonova, E.G. Khaikina. Cryst. Eng. Commun., **26** (3), 277–285 (2024). DOI: 10.1039/D3CE01020A
[10] O.A. Lipina, L.L. Surat, A.Yu. Chufarov, I.V. Baklanova, A.N. Enyashin, M.A. Melkozerova, A.P. Tyutyunnik, V.G. Zubkov. Dalton Trans., **52** (22), 7482–7494 (2023). DOI: 10.1039/D3DT00269A

[11] W. Xu, X. Zhu, D. Zhao, L.J. Zheng, F.K. Shang, Z.G. Zhang. J. Rare Earths, **40** (2), 201–210 (2022). DOI: 10.1016/j.jre.2020.12.011
[12] L. Zhao, B. Lou, J. Mao, B. Jiang, X. Wei, Y. Chen, M. Yin. Mater. Res. Bull., **109**, 103–107 (2019). DOI: 10.1016/j.materresbull.2018.09.032
[13] M. Song, W. Zhao, J. Xue, L. Wang, J. Wang. J. Lumin., **235**, 118014 (2021). DOI: 10.1016/j.jlumin.2021.118014
[14] Y. Gao, F. Huang, H. Lin, J. Zhou, J. Xu, Y. Wang. Adv. Funct. Mater., **26**, 3139–3145 (2016). DOI: 10.1002/adfm.201505332
[15] J. Xue, H.M. Noh, B.C. Choi, S.H. Park, J.H. Kim, J.H. Jeong, P. Du. Chem. Eng. J., **382**, 122861 (2020). DOI: 10.1016/j.cej.2019.122861
[16] Y. Chen, Y. Shen, L. Zhou, J. Lin, J. Fu, Q. Fang, R. Ye, Y. Shen, S. Xu, L. Lei, D. Deng. J. Lumin., **249**, 118995 (2022). DOI: 10.1016/j.jlumin.2022.118995
[17] X. Zhang, Y. Xu, X. Wu, S. Yin, C. Zhong, C. Wang, L. Zhou, H. You. Chem. Eng. J., **481**, 148717 (2024). DOI: 10.1016/j.cej.2024.148717.
[18] Y. Luo, D. Zhang, S. Xu, L. Li, L. Chen, H. Guo. J. Lumin., **257**, 119780 (2023). DOI: 10.1016/j.jlumin.2023.119780
[19] L. Li, X. Tang, Z. Wu, Y. Zheng, S. Jiang, X. Tang, G. Xiang, X. Zhou. J. Alloys Compd., **780**, 266–275 (2019). DOI: 10.1016/j.jallcom.2018.11.378
[20] J. Wang, M. Song, H.J. Seo. J. Lumin., **222**, 117185 (2020). DOI: 10.1016/j.jlumin.2020.117185
[21] D.V.M. Paiva, S.K. Jakka, M.A.S. Silva, J.P.C. Nascimento, M.P.F. Graça, A.S.B. Sombra, M.J. Soares, S.E. Mazzetto, P.B.A. Fechine, K. Pavani. Optik, **246**, 167825–167832 (2021). DOI: 10.1016/j.ijleo.2021.167825
[22] J. Deng, Z. Wang, W. Zhou , M. Yu, J. Min, X. Jiang , Z. Xue, C. Ma, Z. Cheng, G. Luo. Ceram. Int., **49** (9), 14478–14486 (2023). DOI: 10.1016/j.ceramint.2023.01.036
[23] I.E. Kolesnikov, D.V. Mamonova, M.A. Kurochkin, V.A. Medvedev, E.Yu. Kolesnikov. J. Alloys Compd., **922**, 166182 (2022). DOI: 10.1016/j.jallcom.2022.166182
[24] Y. Gao, X. Zhu, H. Shi, P. Jiang, R. Cong, T. Yang. J. Lumin., **242**, 118598 (2022). DOI: 10.1016/j.jlumin.2021.118598
[25] J. Wang, X. Peng, D. Cheng, Z. Zheng, H. Guo. J. Rare Earths, **39** (3), 284–290 (2021). DOI: 10.1016/j.jre.2020.06.010
[26] M. Qu, X. Zhang, X. Mi, H. Sun, Q. Liu, Z. Bai. J. Alloys Compd., **872**, 159506 (2021). DOI: 10.1016/j.jallcom.2021.159506
[27] J. Xie, L. Cheng, H. Tang, Z. Wang, H. Sun, L. Lu, X. Mi, Q. Liu, X. Zhang. Inorg. Chem. Front., **8**, 4517–4527 (2021). DOI: 10.1039/D1QI00831E
[28] A.P. Tyutyunnik, A.Yu. Chufarov, L.L. Surat, O.A. Lipina, V.G. Zubkov. Mendeleev Commun., **28** (6), 661 (2018). DOI: 10.1016/j.mencom.2018.11.035
[29] O.A. Lipina, A.V. Chvanova, M.A. Melkozerova, A.Yu. Chufarov, Y.V. Baklanova, L.L. Surat, A.P. Tyutyunnik, V.G. Zubkov, A.N. Enyashin, L.Yu. Mironov, K.G. Belova. Dalton Trans., **50**, 10935 (2021). DOI: 10.1039/d1dt01780
[30] H. Tang, H. Li, R. Song, Z. Yang, R. Zhao, Z. Guo, J. Li, B. Wang, J. Zhu. Ceram. Int., **49** (19), 31898–31906 (2023). DOI: 10.1016/j.ceramint.2023.07.152
[31] W. Kraus, G. Nolze. J. Appl. Cryst., **29**, 301–303 (1996). DOI: 10.1107/S0021889895014920
[32] R.D. Shannon. Acta Crystallogr. Sect. A Cryst. Phys. Diffr. Theor. Gen. Crystallogr., **32**, 751–767 (1976). DOI: 10.1107/S0567739476001551
[33] Q. Li, L. Jiang, S. Zhu, H. Tang, W. Zhang. J. Mater. Sci.: Materials in Electronics, **29**, 16956–16961 (2018).
[34] Q. Shi, F. You, S. Huang, J. Cui, Y. Huang, Y. Tao. J. Alloys Compd., **654**, 441–444 (2016).
[35] Y.C. Li, Y.S. Chang, Y.C. Lai, Y.J. Lin, C.H. Laing, Y.H. Chang. Mater. Sci. Eng. B, **146**, 225–230 (2008).
[36] Q. Shi, F. You, S. Huang, H. Peng, Y. Huang, Y. Tao. J. Lumin., **152**, 138–141 (2014).
[37] C.S. McCamy. Color Res. Appl., **17**, 42 (1992). DOI: 10.1002/col.5080170211
[38] L. Vijayalakshmi, K. Naveen Kumar, P. Hwang. Scripta Mater., **187**, 97–102 (2020). DOI: 10.1016/j.scriptamat.2020.06.014
[39] Y. Hu, X. Li, K. Wang, Z. Guan, H. Yu, Y. Zhang, S. Xu, B. Chen. J. Lumin., **257**, 119722 (2023). DOI: 10.1016/j.jlumin.2023.119722
[40] O.A. Lipina, A.V. Chvanova, L.L. Surat, Ya.V. Baklanova, A.Yu. Chufarov, A.P. Tyutyunnik, V.G. Zubkov. Dalton Trans., **53**, 7985–7995 (2024). DOI: 10.1039/d4dt00258j
[41] *Encyclopedia of Spectroscopy and Spectrometry*. Eds: J.C. Lindon, G.E. Tranter, D.W. Koppenaal (Elsevier Ltd., 2017).

Translated by E.Ilinskaya